



## Research article

# A novel framework for addressing uncertainties in machine learning-based geospatial approaches for flood prediction

Mohammed Sarfaraz Gani Adnan<sup>a,\*</sup>, Zakaria Shams Siam<sup>d,g</sup>, Irfat Kabir<sup>a</sup>, Zobaidul Kabir<sup>e</sup>, M. Razu Ahmed<sup>f</sup>, Quazi K. Hassan<sup>f</sup>, Rashedur M. Rahman<sup>b</sup>, Ashraf Dewan<sup>c</sup>

<sup>a</sup> Department of Urban and Regional Planning, Chittagong University of Engineering and Technology (CUET), Chattogram, 4349, Bangladesh

<sup>b</sup> Department of Electrical and Computer Engineering, North South University, Dhaka, Bangladesh

<sup>c</sup> Spatial Sciences Discipline, School of Earth and Planetary Sciences, Curtin University, Perth, 6102, Australia

<sup>d</sup> Department of Electrical and Computer Engineering, Presidency University, Dhaka, Bangladesh

<sup>e</sup> School of Environmental and Life Sciences University of Newcastle NSW-2258, Australia

<sup>f</sup> Department of Geomatics Engineering, University of Calgary, 2500 University Drive NW, Calgary, Alberta, T2N 1N4, Canada

<sup>g</sup> Department of Electrical, Electronic and Systems Engineering, Faculty of Engineering and Built Environment, Universiti Kebangsaan Malaysia, 43600, Bangi, Selangor, Malaysia



## ARTICLE INFO

## Keywords:

Flood susceptibility  
Machine learning algorithm  
Uncertainty analysis  
GIS  
Remote sensing

## ABSTRACT

Globally, many studies on machine learning (ML)-based flood susceptibility modeling have been carried out in recent years. While majority of those models produce reasonably accurate flood predictions, the outcomes are subject to uncertainty since flood susceptibility models (FSMs) may produce varying spatial predictions. However, there have not been many attempts to address these uncertainties because identifying spatial agreement in flood projections is a complex process. This study presents a framework for reducing spatial disagreement among four standalone and hybridized ML-based FSMs: random forest (RF), k-nearest neighbor (KNN), multilayer perceptron (MLP), and hybridized genetic algorithm-gaussian radial basis function-support vector regression (GA-RBF-SVR). Besides, an optimized model was developed combining the outcomes of those four models. The southwest coastal region of Bangladesh was selected as the case area. A comparable percentage of flood potential area (approximately 60% of the total land areas) was produced by all ML-based models. Despite achieving high prediction accuracy, spatial discrepancy in the model outcomes was observed, with pixel-wise correlation coefficients across different models ranging from 0.62 to 0.91. The optimized model exhibited high prediction accuracy and improved spatial agreement by reducing the number of classification errors. The framework presented in this study might aid in the formulation of risk-based development plans and enhancement of current early warning systems.

## 1. Introduction

Natural hazards like floods have become more frequent in recent decades, endangering human lives, property, agriculture, urban infrastructure, and socioeconomic conditions. Floods are projected to occur more frequently and with greater intensity due to unprecedented changes in the climate (Falah et al., 2019; Khosravi et al., 2019; Msabi and Makonyo, 2021). Traditional flood management strategies involved the construction of structural measures to reduce risk associated with floods. However, structural flood protection measures could encourage

floodplain development by engendering a sense of safety (Di Baldassarre et al., 2013; Montz and Tobin, 2008). Therefore, the failure of structural flood interventions may exacerbate flood damages (Hui et al., 2016).

A risk-based approach to flood management, which includes flood prediction and early warning system, has become the paradigm for flood control methods (Poussin et al., 2015). Accurate flood forecasting is essential for avoiding or reducing the effects of possible threats (Papaioannou et al., 2018). To forecast floods, both deterministic and probabilistic approaches are used (Apel et al., 2009; Di Baldassarre et al., 2010). The deterministic approach to floodplain mapping includes the use of various hydrodynamic physical flood models such as HEC-RAS

\* Corresponding author.

E-mail addresses: [sarfarazadnan@cuet.ac.bd](mailto:sarfarazadnan@cuet.ac.bd) (M.S.G. Adnan), [zakaria.siam@northsouth.edu](mailto:zakaria.siam@northsouth.edu) (Z.S. Siam), [irfatkabir@gmail.com](mailto:irfatkabir@gmail.com) (I. Kabir), [Zobaidul.Kabir@newcastle.edu.au](mailto:Zobaidul.Kabir@newcastle.edu.au) (Z. Kabir), [mohammad.ahmed2@ucalgary.ca](mailto:mohammad.ahmed2@ucalgary.ca) (M.R. Ahmed), [qhassan@ucalgary.ca](mailto:qhassan@ucalgary.ca) (Q.K. Hassan), [rashedur.rahman@northsouth.edu](mailto:rashedur.rahman@northsouth.edu) (R.M. Rahman), [A.Dewan@curtin.edu.au](mailto:A.Dewan@curtin.edu.au) (A. Dewan).

<https://doi.org/10.1016/j.jenvman.2022.116813>

Received 20 May 2022; Received in revised form 29 October 2022; Accepted 14 November 2022

Available online 23 November 2022

0301-4797/© 2022 The Authors. Published by Elsevier Ltd. This is an open access article under the CC BY license (<http://creativecommons.org/licenses/by/4.0/>).

Abbreviation description			
AHP	Analytic Hierarchy Process	KNN	k-nearest neighbor
ALOS	Advanced Land Observing Satellite	ML	Machine learning
AUC	Area under the receiver operating characteristic curves	MLP	Multilayer perceptron
BARC	Bangladesh Agricultural Research Council	MSE	Mean squared error
BMD	Bangladesh Meteorological Department	NPV	Negative predictive value
CEP	Coastal Embankment Project	OA	Overall accuracy
DEM	Digital Elevation Model	PPV	Positive predictive value
FSM	Flood susceptibility model	RF	Random forest
GA	Genetic algorithm	ROC	Receiver operating characteristic curves
GA-RBF-SVR	Genetic algorithm-gaussian radial basis function-support vector regression	SAR	Synthetic aperture radar
GIS	Geographic Information Systems	SPI	Stream Power Index
		SVM	Support vector machine
		TWI	Topographic Wetness Index
		VIF	Variance inflation factors

(Ardiclioglu et al., 2022; Brunner, 1995) and MIKE (Zhou et al., 2012), and Delft3D-FLOW (Muñoz et al., 2021) models, which aim to establish the relationship between rainfall and runoff to predict inundations. But these physical models are data-intensive and may have significant uncertainties, especially when water flows are projected beyond the observation intervals (Di Baldassarre et al., 2010).

Floodplain mapping is challenging as floods are the result of complex interactions between a variety of factors related to hydro-meteorology, topography, and anthropogenic environments (Bui et al., 2016; Khosravi et al., 2019). To address this challenge, flood susceptibility mapping has been proved to be effective in identifying areas prone to flooding (Bui et al., 2016; Kjeldsen, 2010; Malik and Pal, 2021; Mansur et al., 2018). The advancement of geospatial technologies (e.g., Geographic Information Systems (GIS) and remote sensing) have made important contributions to hydrological research in recent decades, by providing continuous data for flood forecasting and risk assessment (Haq et al., 2012; Tehrany et al., 2014b; Dewan et al., 2006). A finer spatial and temporal resolution of remotely sensed data has provided researchers with access to historical soil, geomorphological, and hydrological profiles of floodplains that are essential factors for flood susceptibility mapping (Haq et al., 2012; Kalantar et al., 2021; Msabi and Makonyo, 2021; Tralli et al., 2005; Wang et al., 2019).

To map flood susceptibility, researchers used both qualitative and quantitative methods (Msabi and Makonyo, 2021; Shafizadeh-Moghadam et al., 2018). The Analytic Hierarchy Process (AHP) is one of the qualitative methods for flood susceptibility mapping (Vojtek and Vojteková, 2019). Quantitative approaches can however be classified into two categories: statistical and machine learning-based approaches. Numerous statistical techniques have been used to predict floods over the years. Examples include the use of weights of evidence (Batar and Watanabe, 2021; Costache, 2019; Tehrany et al., 2014b), bivariate (Ali et al., 2020; Tehrany et al., 2013, 2014a) and multivariate approaches (Al-Juaidi et al., 2018; Tehrany et al., 2013, 2014a). However, statistical models were criticized for failing to capture the nonlinear relationships between flood episodes and their underlying causes (Bui et al., 2019; Khosravi et al., 2019; Nachappa et al., 2020).

Machine learning (ML)-based models have gained increased attention for flood forecasting in recent years due to their ability to handle large amounts of data and comprehend nonlinear relationships between floods and their indicators (Bui et al., 2019; Khosravi et al., 2019; Nachappa et al., 2020; Shahabi et al., 2020). Researchers employed both standalone and hybridized ML algorithms to determine flood susceptibility (Rahman et al., 2019; Siam et al., 2021). Traditional ML models are artificial neural networks (ANNs) in the form of Multi-Layer Perceptrons (MLPs) (Kia et al., 2012; Rezaeianzadeh et al., 2014; Youssef et al., 2011), support vector machine (SVM) (Islam et al., 2021; Nachappa et al., 2020; Tehrany et al., 2019), wavelet-based artificial neural network (Kumar et al., 2022), as well as nonparametric

algorithms like k-nearest neighbor (KNN) (He and Wang, 2007; Liu et al., 2016; Shahabi et al., 2020), and Random Forest (RF) (Chen et al., 2020; Lee et al., 2017). In addition, several hybridized ML models for flood prediction have been developed (Siam et al., 2021). Evidence from several works suggested that hybridized models are superior to stand-alone models in terms of accuracy and robustness (Rahman et al., 2019; Siam et al., 2021).

Although a large number of standalone and hybridized ML-based FSMs have been developed, uncertainties may exist in the resultant floodplain maps. The choice of modeling approach could be a major source of uncertainty since each model responds to geographical region and sample size differently (Shafizadeh-Moghadam et al., 2018). Uncertainties may also arise due to: (1) spatial heterogeneity of the land surface (Zhao et al., 2019), (2) a lack of historical flood observation data (Adnan et al., 2020b), (3) complexities in selecting an optimal combination of models (Shafizadeh-Moghadam et al., 2018; Shahabi et al., 2020), (4) choice of input parameters (Shirzadi et al., 2020), (5) error in data (e.g., incorrect flood labels) (Crosetto et al., 2000), (6) inadequate sampling resolution (Avand et al., 2022; Crosetto et al., 2000; Saha et al., 2021), (7) dependency on experts' opinions (e.g., knowledge-based methods) (Nachappa et al., 2020), and (8) combining heterogeneous models (Zhao et al., 2019).

The majority of the existing studies on FSM focused on comparing several ML techniques in order to select the most accurate model. FSMs are often assessed using receiver operating characteristic curves (ROC), the non-parametric Freidman test, the Wilcoxon signed-rank test, statistical evaluation measures (such as overall accuracy, the kappa statistic, and root-mean-square error), and other performance indicators (El-Haddad et al., 2021; Shafizadeh-Moghadam et al., 2018). The ROC is a common form of model performance assessment indicator that provides a comprehensive, informative, and visually appealing measure of accuracy (Tehrany et al., 2013). Such a method consists of two elements: establishing the model and comparing projected maps with independently observed data sets. But utilizing the aforementioned methods to choose the best model when several models perform similarly is neither an easy task nor even feasible. It is possible for two or more susceptibility maps with similar accuracy and prediction capabilities to differ spatially in terms of the heterogeneity of the predicted spatial pattern (Adnan et al., 2020a; Sterlacchini et al., 2011).

Despite producing high prediction accuracy, recent studies were unable to adequately explain the pixel-by-pixel agreement<sup>1</sup> across susceptibility maps created using various flood prediction models (Dasgupta et al., 2018; Löwe et al., 2021; Sarker et al., 2019). Less attention

<sup>1</sup> In this study, "spatial agreement" refers to a high level of pixel-by-pixel correlation between the locations of the observed and modeled floods, whereas "spatial disagreement" is indicated by low correlation coefficients.

is given to investigate and improve spatial agreement among susceptibility maps generated by various models utilizing various ML-based models. To address the challenges noted above, this study proposes a method to minimize uncertainty in predicted spatial patterns in ML-based FSM. Therefore, two objectives were formulated: (1) to determine the degree of spatial agreement between four standalone and hybridized ML-based FSMs — RF, KNN, MLP, and GA-RBF-SVR; (2) to develop a regression-based FSM incorporating the outcomes of those four models to improve predicted spatial pattern. The study utilized the southwest coastal region of Bangladesh as a case, which is prone to multiple types of flooding (Adnan et al., 2019).

## 2. Materials and methods

This study includes five methodological steps: (1) observing flood events to develop a flood inventory map, (2) selecting flood causative factors, (3) developing FSMs, (4) identifying spatial dis (agreement) among various ML-based models, and (5) developing a framework to improve spatial agreement in FSMs. Fig. 1 shows an overview of the methodology followed in this study.

### 2.1. Study area

The study focused on Bangladesh's southwestern coastal region (Fig. 2), which is vulnerable to several forms of flooding, including pluvial flooding, tidal flooding, and storm surges brought on by tropical cyclones (Adnan et al., 2019). The heavily engineered coastal region consists of 139 polders (a Dutch term describing enclosed coastal embankments). This study focused on 44 polders crisscrossed over five southwest coastal districts — Bagerhat, Jessore, Khulna, Pirojpur, and Satkhira — home to approximately 5.3 million people (Bondarenko et al., 2020). The area is approximately 5187 km<sup>2</sup> in size, with a mean elevation of 3.2 m. The construction of polders in this region began in the 1960s as part of a major Coastal Embankment Project (CEP) (Ali, 2002; Mirza and Ericksen, 1996). The CEP was designed to protect agricultural lands against saline intrusion, tidal flooding, and storm surge induced flooding (Warner et al., 2018). A series of polders were constructed in the coastal region from the 1960s to the 1980s (Adnan et al., 2020b).

The initial success of polders construction in increasing agricultural productivity was hindered by geomorphological changes in the embanked region caused by the separation of floodplains from adjacent rivers. The embanked region has experienced both riverbed siltation, which lowers rivers' capacity to retain water, and land subsidence (i.e., settling or sinking of the Earth's surface), which encouraged surface depressions. The rate of land subsidence in the coastal region is, on average, roughly 2–3 mm/year (Brown and Nicholls, 2015). Besides, inadequate and depleted drainage systems have resulted in temporary or permanent waterlogging in a number of locations (Adnan et al., 2019; Auerbach et al., 2015). While a few studies attempted to develop deterministic (Haque et al., 2018) or probabilistic (Adnan et al., 2020b) flood models to simulate pluvial and/or tidal floods in the study area, uncertainties in those models are not well understood.

### 2.2. Flood inventory mapping

FSMs hypothesize that the likelihood of an area being inundated depends on a similar set of flood causative factors explicating inundations during historical events. Thus, the accuracy of FSMs depends on the accuracy of historical flood observation data (Nachappa et al., 2020). This study utilized a flood inventory map created by Adnan et al. (2020b), which was based on historical flood observations from 1988 to 2012 that were generated from satellite data. The inventory map showed the ratio of the number of times a region flooded to the total number of observation years, which is referred to as "flood frequency". The flood inventory map was used to determine random flood and

non-flood locations (Tehrany et al., 2019). Using the flood inventory map, a total of 1000 random locations were generated, whereby flood and non-flood locations were 586 and 414, respectively (Fig. 2).

### 2.3. Flood causative factors

The choice of flood conditioning factors is crucial for the accurate mapping of flood susceptibility. The existing studies used diverse flood indicators (Khosravi et al., 2019; Nachappa et al., 2020; Tehrany et al., 2019). Based on relevant literature review and with regard to local characteristics, this study selected 14 flood conditioning factors, classified under five broad categories: topographical, hydrometeorological, anthropogenic, geological, and locational factors. Raster images of all 14 factors were created at 30 m spatial resolution. Data sources of all flood conditioning factors are given in Table 1.

Topographical factors included aspect, elevation, curvature, slope, and land subsidence (Fig. S1, Supplementary document). This study utilized Advanced Land Observing Satellite (ALOS) Digital Elevation Model (DEM) (JAXA, 2015) to develop raster layers of aspect, elevation, curvature, and slope. Aspect is a crucial component of flood susceptibility mapping, which describes slope's orientation and the amount of precipitation and sunshine that an area is likely to receive (Nachappa et al., 2020). Surface elevation is considered to be one of the most important indicators of flooding since water usually flows from high to lowlands. Besides, elevation influences on other topographical features such as aspect, slope, and curvature (Khosravi et al., 2019). In the case of curvature, flat or concave surfaces are primarily susceptible to flooding (Tehrany et al., 2014b). Slope controls flooding by regulating the speed of surface runoff velocity and vertical percolation. Areas with lower slopes are typically more vulnerable to flooding (Youssef et al., 2011). Land subsidence is a significant cause of pluvial flooding in coastal Bangladesh (Brown and Nicholls, 2015). Land subsidence layer used in this study was obtained from Adnan et al. (2020b), who estimated subsidence in the southwest embanked region using 205 training measurement points turned into a raster layer using the natural neighbor interpolation method.

Four hydrometeorological factors were considered in this study: precipitation, Stream Power Index (SPI), flow accumulation, and the Topographic Wetness Index (TWI) (Supplementary document, Fig. S2). An annual mean precipitation layer was created using 10-day gridded precipitation data from the Bangladesh Meteorological Department (BMD) from 1948 to 2012. SPI, TWI, and flow accumulation indicate the natural drainage characteristics of the study area. Flow accumulation explains cumulative volumes of water moving downslope. A flow accumulation layer was developed from a continuous drainage network developed from DEM (Tehrany et al., 2014b). The SPI illustrates the erosive impact of surface runoff (Nachappa et al., 2020). Significantly high SPI areas are more likely to experience flooding (Bannari et al., 2017). TWI shows the amount of flow collecting at any point while taking gravity-driven downstream flow trends into account. It describes how wet a location is in relation to its surroundings (Khosravi et al., 2019). The following equations were used to develop gridded data for SPI and TWI.

$$SPI = A_s \times \tan \beta \quad (1)$$

$$TWI = \ln \left( \frac{A_s}{\tan \beta} \right) \quad (2)$$

where  $A_s$  and  $\beta$  are the specific catchment area (m<sup>2</sup>/m) and slope gradient, respectively.

This work also selected five variables related to anthropogenic (land use), geological (soil texture and soil permeability), and locational (distance to adjacent rivers and drainage channels) characteristics of the study area (Fig. S3, Supplementary document). The pattern of land use in an area affects evapotranspiration, which measures the amount of

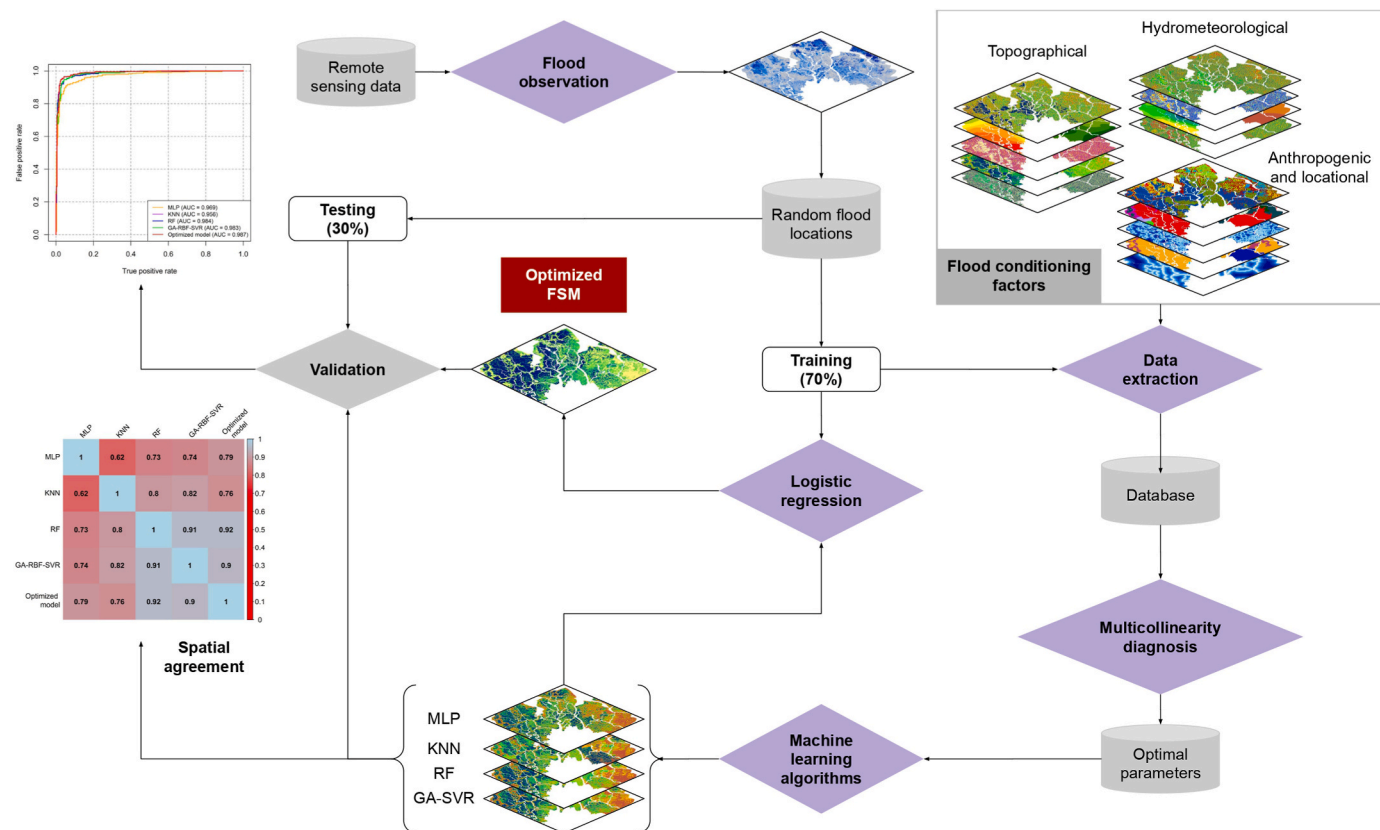


Fig. 1. Methodological flow of the study.

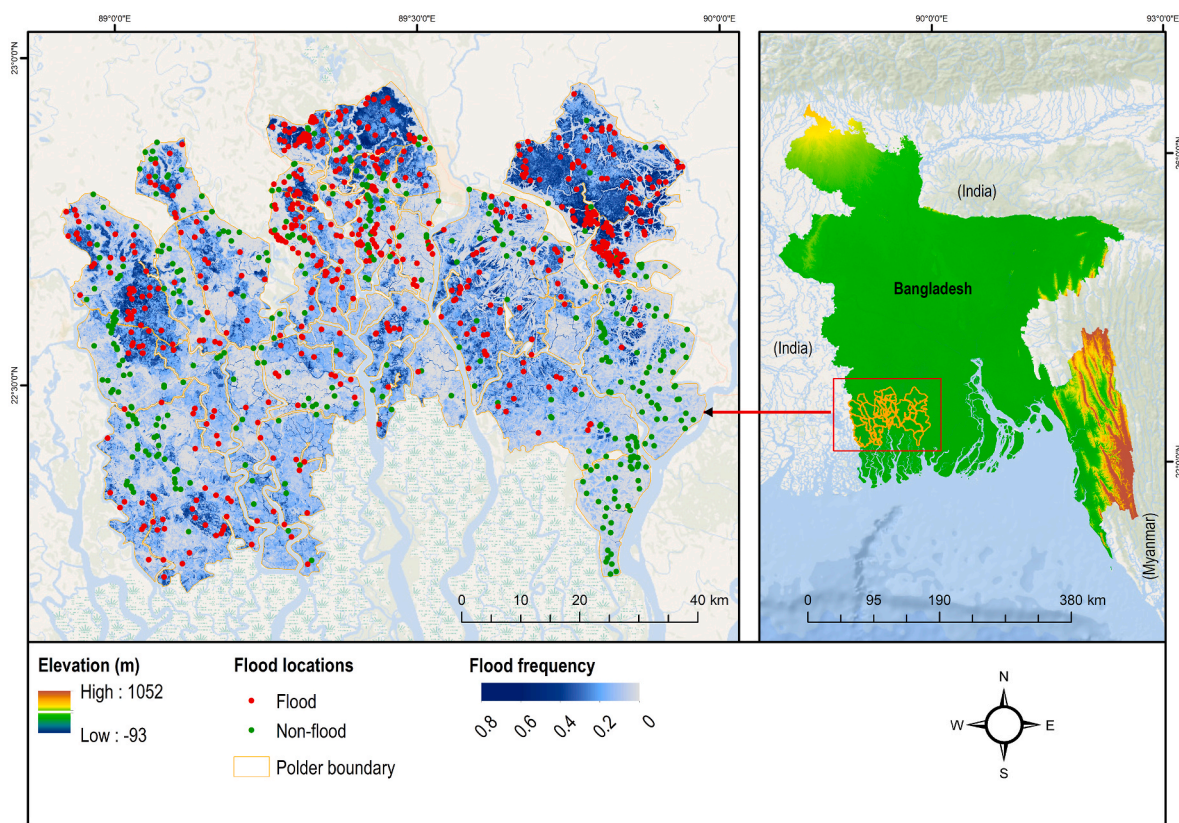


Fig. 2. Location map of southwest embanked region of Bangladesh, with sample flood and non-flood points.

**Table 1**

Flood conditioning factors used in this study.

No.	Conditioning factor	Data type	Data Source	VIF (Iteration 1)	VIF (Iteration 2)
1	Aspect	Continuous	Estimated from DEM	1.09	1.03
2	Elevation	"	DEM (JAXA, 2015)	2.15	2.11
3	Slope	"	Estimated from DEM	2.08	1.19
4	Curvature	Discrete	"	1.61	1.46
5	Land subsidence	Continuous	Adnan et al. (2019)	1.57	1.56
6	Precipitation	"	<a href="http://www.bmd.gov.bd">http://www.bmd.gov.bd</a>	2.33	2.32
7	Flow accumulation	"	Estimated from DEM	8.76	–
8	SPI	"	"	6.88	1.34
9	TWI	"	"	11.75	–
10	Land cover	Discrete	Mukhopadhyay et al. (2018)	1.34	1.31
11	Soil texture	"	<a href="http://www.barc.gov.bd/">http://www.barc.gov.bd/</a>	1.23	1.23
12	Soil permeability	"	"	1.51	1.50
13	Distance to drainage channels	Continuous	Adnan et al. (2019)	1.09	1.09
14	Distance to rivers	"	WARPO (2018)	1.11	1.10

runoff and its velocity (Tehrany et al., 2019). Land use data utilized in this study was collected from Mukhopadhyay et al. (2018) that included 12 classes (Fig. S3 (a)). Topsoil texture and soil permeability are two geological factors that determine the degree of infiltration. These datasets were collected from Bangladesh Agricultural Research Council (BARC). The characteristics of soil and land use of an area determine water balance (Tehrany et al., 2019). The polders in coastal Bangladesh are connected to many drainage channels and sluice gates to prevent saltwater intrusion during the dry season and drain surplus runoff during the wet season. A study by Adnan et al. (2020b) exhibited that the distance between an area and nearby drainage channels and rivers can be a good indicator of how susceptible it is to flooding. This study created two raster layers using the Euclidean distance algorithm to compute the distance between a particular location and neighboring drainage systems. Vector data of drainage channels were collected from Adnan et al. (2019).

#### 2.4. Multicollinearity analysis to select optimum number of factors

In order to avoid flood conditioning factors that are susceptible to multicollinearity, this study evaluated variance inflation factors (VIF). It is a method that is frequently employed to assess the multi-collinearity of flood conditioning parameters (Yariyan et al., 2020). When a variable's VIF value is  $> 2.5$ , bias is introduced into the model, and when it is  $> 10$ , multicollinearity is present (Midi et al., 2010). For the purposes of this study, factors with VIF values under 2.5 were chosen for modeling flood susceptibility. From 14 flood conditioning factors, 12 were included in the modeling purposes since the addition of TWI and flow accumulation greatly enhanced VIF values (Table 1).

#### 2.5. Data preprocessing

Values of each of the 12 flood conditioning factors were extracted at random flood locations using GIS. The resulting dataset did, however, contain some missing values, which were pruned. Subsequently, 965 samples altogether were used for to create the models. The models were created utilizing 70% of the total samples for training and the rest 30% for testing, which is consistent with previous studies (Pham et al., 2021; Tehrany et al., 2019). Finally, there were 675 training samples and 290 test samples, respectively. The training samples' corresponding ratios of flood and non-flood locations were 401 and 274. According to Islam et al. (2021), there should be a similar number of flood and non-flood samples to minimize bias. Therefore, the minority class — the non-flood class — was oversampled using the 'ovun.sample' function of the random over-sampling examples (ROSE) package in R. Consequently, oversampled train dataset contained a total of 389 non-flood and 401 flood locations.

Several flood conditioning factors selected in this study have physical dimensions. Equation (3) shows how all continuous variables were

scaled using the z-score normalization technique to eliminate the physical dimensions. The ranges of each flood conditioning factor within the training and test datasets, respectively, before and after scaling are shown in the supplemental material (Table S1 and Table S2).

$$z = \frac{x - \mu}{\sigma} \quad (3)$$

where  $\mu$  and  $\sigma$  are the mean and standard deviation of a feature vector.

#### 2.6. Flood susceptibility mapping

This study developed four supervised machine learning models for mapping flood susceptibility: random forest, k-nearest neighbor, multilayer perceptron, and hybridized genetic algorithm-gaussian radial basis function-support vector regression (GA-RBF-SVR). Equation (4) was used to estimate flood susceptibility scores (FS) on a pixel-by-pixel basis (Siam et al., 2021).

$$FS = \sum_{m=1}^n w_m x_m \quad (4)$$

where  $n$  is the number of flood conditioning factors,  $x_m$  is the flood conditioning factors, and  $w_m$  is the weight of each factor.

##### 2.6.1. Multilayer perceptron (MLP)

The Multilayer perceptron (MLP), one of the most widely used supervised machine learning models, offers a fundamental feedforward neural network architecture that can be applied for both classification and regression (Murtagh, 1991). This model consists of a single input layer, several hidden layers, and an output layer. The output of an input layer was sent as an input into the following layer. The procedure is repeated until the last hidden layer is reached. Several weights and biases in the model need to be adjusted throughout the training process. In this study, the Resilient Backpropagation algorithm (RPROP+) was used to train the MLP model to acquire the optimal weights and biases. Two hidden layers were used where the first and second layers included ten and three nodes, respectively. The maximum step for training was set at 106, and the threshold was set at 0.1. The MLP model was applied using the R 'neuralnet' library. The results of an MLP model vary from run to run because the input parameters can give various initial weights, which is one of its drawbacks (Ahmadlou et al., 2021). To address this issue, the model was iterated multiple times, and the model with the highest accuracy was chosen as the final.

##### 2.6.2. K-nearest neighbor (KNN)

The k-nearest neighbor (KNN) is a supervised machine learning technique that utilizes the proximity or vicinity of data points or samples, presuming that similar things are close to one other (Cover and Hart, 1967). The KNN model uses "feature similarity" to predict the

values of novel samples or data points. The novel sample is consequently assigned a value based on how similar it is to the sample in the training set. The distance function, which determines  $k$  neighbor samples or data points in the train set that are closest to the input, defines the proximity. The input label was predicted over the labels of the  $k$  samples or data points using the ‘majority-vote’ method. As a result, the model gets less sensitive to noise as  $k$  grows. Because KNN classifiers depend on every sample in the entire training set, their performance is computing intensive (Shahabi et al., 2020). This study utilized the Euclidean distance algorithm as a distance function. Since  $k$  is a hyperparameter, the model used different values of it. This study noted that the model performed better when the value of  $k$  was set to five. The ‘knnreg’ function of ‘caret’ package in the R language was used to implement the KNN model.

### 2.6.3. Random forest (RF)

Random forest (RF) (Breiman, 2001) is one of the most popular supervised machine learning models for solving classification and regression problems. The model creates a number of decision trees using training data. In order to achieve a greater accuracy or a minimum error, each decision tree generates an output, and the final output is produced by majority voting or averaging at the time of inference for classification and regression, respectively. RF does have certain limitations, especially when there are many trees included in the model. The computation becomes inefficient and slow as a result (Zhu and Zhang, 2022). This study used the ‘randomForest’ package in R to implement this algorithm. In order to improve model performance, the number of ‘trees’ was set to be 500, and three variables were randomly picked as candidates at each internal node in the tree. The parameter ‘cross’ was set to a value of 10 to apply a 10-fold cross-validation approach on the training dataset to subdue bias.

### 2.6.4. Hybridized GA-RBF-SVR model

A hybridized genetic algorithm – gaussian radial basis function – support vector regression (GA – Gaussian RBF – SVR) model was also developed in this study to map flood susceptibility. The SVR is a widely used algorithm in flood susceptibility mapping that can define the relationship between the input and output data using equation (5).

$$f(x) = w^T \psi(x) + bias \quad (5)$$

where  $x \in R^n$  is the flood causative features,  $w \in R^n$  is the weight vector, and  $\psi(x)$  is the non-linear mapping function. Equation (6) exhibits the final solution to the constrained optimization problem in SVR utilizing the Lagrangian formulation.

$$f(x) = \sum_{j=1}^n (\alpha_j - \alpha_j^*) k(x, x_j) + bias \quad (6)$$

where  $\alpha_j$  and  $\alpha_j^*$  are the Lagrangian multipliers and  $k(x_m, x_n) = \langle \psi(x_m), \psi(x_n) \rangle$  denotes kernel function. Different types of kernels can be applied. This study however used the gaussian radial basis function (gaussian RBF) (equation (7)).

$$k(x, x_j) = e^{-\gamma \|x - x_j\|^2} \quad (7)$$

where  $\gamma$  denotes the spread of the kernel,  $\epsilon$  (epsilon) is the approximation quality and the cost value which regulates the tradeoff between training error and model complexity. This study optimized these three parameters of the gaussian RBF-SVR model utilizing a genetic algorithm (GA). The objective function of GA was defined to be the negative quantity of the mean squared error (MSE) value on the test set prediction. Again, a 10-fold cross-validation technique was applied while training all the SVR models with different values of the parameters on the train set to circumvent overfitting. The model complexity was also evaluated in terms of the number of support vectors in order to model the train set.

This study implemented the GA-Gaussian RBF-SVR model using the ‘ksvm’ function of ‘kernlab’ package in R. ‘Epsilon regression’ was chosen as the function, and the value of ‘cross’ at 10. The kernel was set to ‘rbfdot’ in order to use the gaussian radial basis function kernel. The genetic algorithm was implemented utilizing the ‘ga’ function of the ‘GA’ package in R.

### 2.6.5. Sensitivity analysis and validation of flood susceptibility models (FSMs)

In order to determine the best-performing FSM, this study calculated a number of cutoff-dependent and cutoff-independent validation indicators, including receiver operating characteristic (ROC) and area under the receiver operating characteristic (AUC) curves, overall accuracy (OA), mean squared error (MSE), kappa statistic, positive predictive value (PPV), negative predictive value (NPV), sensitivity and specificity. Using Youden’s index, the optimal cutoff value for binarizing flood susceptibility scores predicted by the models was determined (Youden, 1950). This was accomplished using the ‘optimal.cutpoints’ function in the R package ‘OptimalCutpoints’. The ‘roc’ and ‘plot.roc’ functions of the ‘pROC’ package were used to estimate the values of AUC.

As part of the sensitivity analysis, the importance rank (%IncMSE and IncNodePurity) of each flood conditioning factor was estimated using the RF algorithm. The %IncMSE quantifies the proliferation in the mean squared error value of model prediction when the feature values get randomly permuted. The IncNodePurity metric measures the total curtailment of node impurities anticipated by the Gini Index that is averaged over each of the decision trees. Node impurities were predicted by the Gini Index via variable splitting. The higher values of %IncMSE and IncNodePurity indicators suggest that the model should place more emphasis on certain features and be more sensitive (Siam et al., 2021, 2022).

### 2.7. Identification of uncertainties in flood susceptibility maps

To investigate uncertainties in the inter-model agreeability, pairwise flood susceptibility maps, developed using four standalone and hybridized algorithms, were compared. Pearson’s correlation coefficient was derived to investigate the extent of pixel-wise agreement between the six possible combinations of FSMs. The estimated correlation coefficient indicates the covariance of flood predictions, obtained by using two models, divided by the product of their standard deviations. The correlation coefficient can be anything from +1 to –1, with 0 denoting complete disagreement, 0 to  $\pm 0.29$  as low,  $\pm 0.30$  to  $\pm 0.49$  as moderate,  $\pm 0.50$  to  $\pm 1$  as high, and  $\pm 1$  as perfect agreement. This method evaluates uncertainties between several models, but it does not provide information about inaccuracy in the estimation of the probability of a flood.

### 2.8. Calibrating optimized FSM

This study hypothesized that there are spatial inconsistencies in flood susceptibility maps developed using various combinations of ML models. Therefore, an optimized flood prediction map that integrated four susceptibility maps was developed to address uncertainties in various models. The optimized model was developed by adopting a strategy suggested by Adnan et al. (2020a) and Rossi et al. (2010). A logistic regression (LR) model was established that incorporated binary flood and non-flood locations (see section 2.2) as a dependent variable and the susceptibility scores of four standalone and hybridized ML models as independent variables. The regression coefficients obtained from the LR model were incorporated in Equation (8) to estimate optimized flood susceptibility scores (P) in the study area.

$$P = \frac{1}{1 + e^{-z}} \quad (8)$$

where  $z$  is the linear combination of flood causative factors, which was estimated using the following equation:

$$z = \theta_0 + \theta_1x_1 + \theta_2x_2 + \dots + \theta_nx_n \tag{9}$$

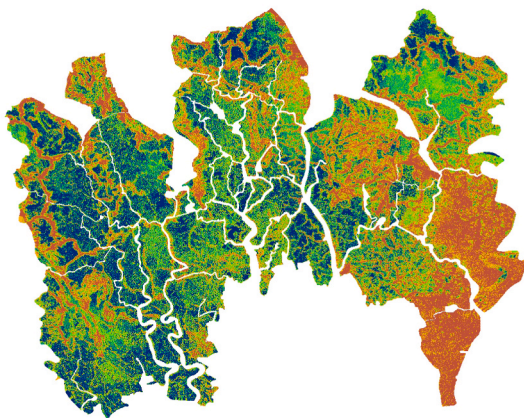
where  $\theta_0$  is the model intercept,  $\theta_i$  ( $i = 1, 2, \dots, n$ ) represents the regression coefficients of independent variables,  $n$  is the number of flood causative factors, and  $x_i$  ( $i = 1, 2, \dots, n$ ) indicates the value of different independent variables. The sensitivity and validation of the optimized FSM were carried out using methods described in section 2.6.5.

### 3. Results

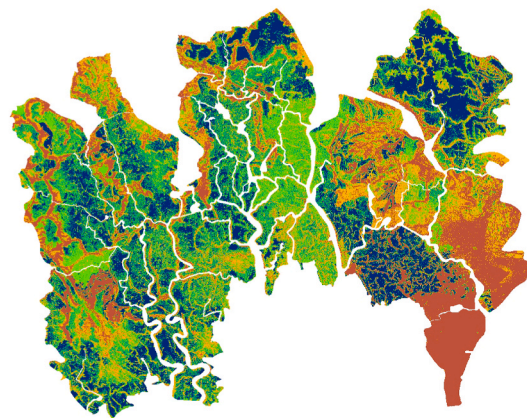
#### 3.1. Flood potential areas

Fig. 3 shows flood susceptibility maps of the southwestern embanked region of Bangladesh developed by using four standalone and hybridized algorithms. The flood potential zones were categorized into five classes using the quantile classification method. The results indicated that most of the areas are susceptible to floods, which can range in severity from moderate to extreme (Fig. 3). Significantly lower variability in the proportion of flood susceptible areas was observed within four standalone and hybridized ML models, with flood susceptible zones ranging from 59.7% to 59.9% of the total area (Fig. 4). The spatial distribution of flood potential zones, however, showed considerable variances (Fig. 3), indicating the presence of uncertainties in different models.

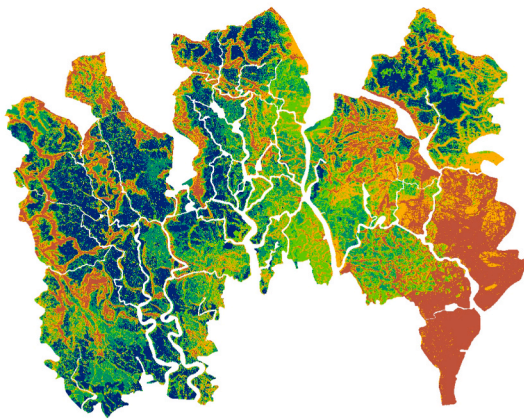
a) MLP



b) KNN



c) RF



d) GA-RBF-SVR

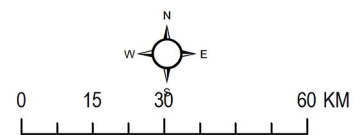
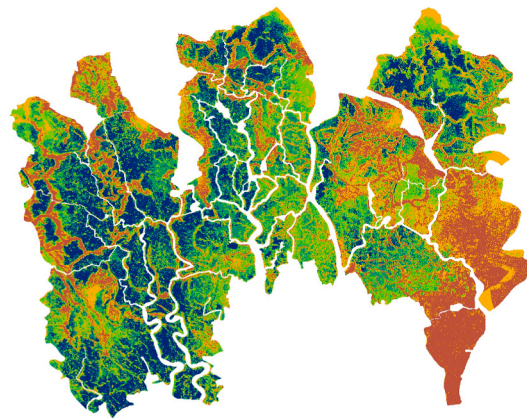


Fig. 3. Flood susceptibility maps, obtained by four machine learning algorithms: (a) Multi-Layer Perceptron (MLP), (b) K-Nearest Neighbor (KNN), (c) Random Forest (RF), and (d) Gaussian approximation and Support Vector Regression (GA-SVR).

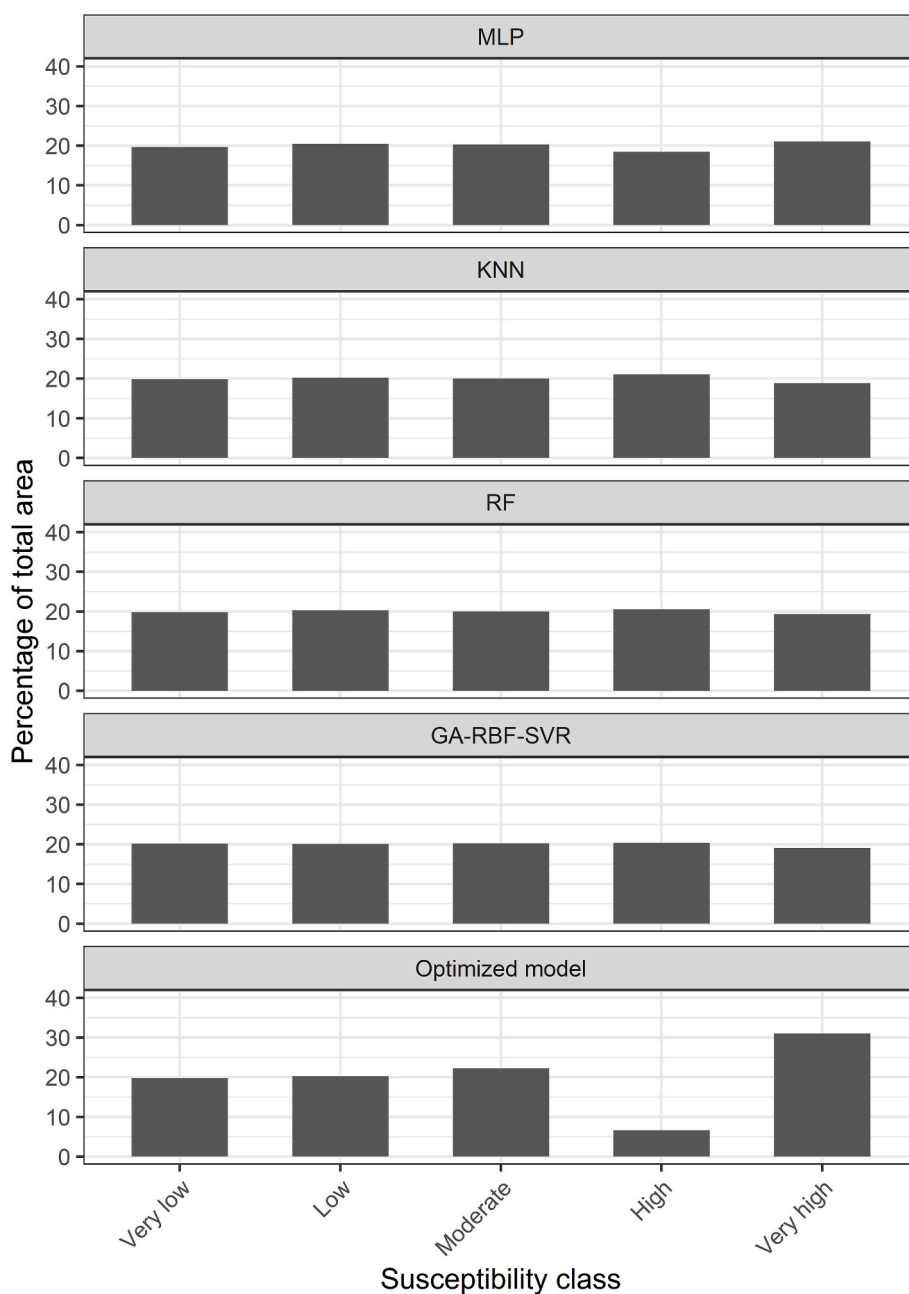


Fig. 4. Flood susceptible areas derived via five models: MLP, KNN, RF, GA-RBF-SVR, and optimized model.

### 3.2. Spatial agreement between various FSMs

In order to assess pixel-level flood probabilities between different FSMs and determine the degree of geographic agreement between them, this study used the Pearson correlation coefficients (Fig. 5). The findings revealed that there was a significant variation in the spatial agreement between FSMs created using four standalone and hybridized ML models, with pair-wise correlation coefficients ranging from 0.62 to 0.91. The hybridized GA-RBF-SVR model generally exhibited a better level of spatial agreement with other models, whereas the KNN model produced the lowest agreement. The GA-RBF-SVR and RF models had the highest correlation coefficient of 0.91 among the four models, whilst the MLP-KNN models had the lowest correlation coefficient value of 0.62.

### 3.3. The optimized FSM

This study developed an optimized FSM model by using the best-predicted pixels from different ML models to address uncertainty regarding spatial disagreement between the models. A multivariate LR model was established utilizing binary flood and non-flood locations as the dependent variable and estimated flood probabilities based on the four standalone and hybridized ML models as independent variables. Table 2 provides an overview of the results of the optimized model. The association between observed flood and non-flood locations and flood probabilities calculated using all four models was statistically significant ( $p$ -value < 0.05). With the coefficient of determinants ( $R^2$ ) of 0.81, the model showed its robustness in predicting flood inventories. Flood probabilities obtained by the KNN model were found to be negatively associated with flood locations. In relation to estimated regression coefficients, the GA-RBF-SVR model had the highest influence on the



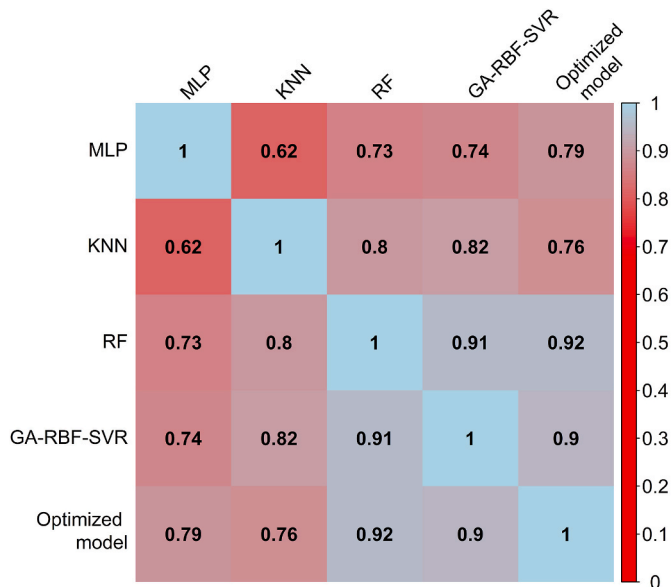


Fig. 5. Correlogram, showing spatial agreement between the five flood susceptibility models.

Table 2  
Parameters and estimates of the optimized flood susceptibility model.

Variables	Coefficients	Standard error	z-value	p-value
Model intercept	-8.46213	0.96268	-8.7902	<2.2e-16 ***
GA-RBF-SVR	9.30307	2.74787	3.3856	0.0007104 ***
KNN	-1.66782	0.82107	-2.0313	0.0422262 *
RF	7.76560	1.53413	5.0619	4.151e-07 ***
MLP	4.26948	1.71665	2.4871	0.0128788 *

Significance codes: 0 '\*\*\*' 0.001 '\*\*' 0.01 '\*' 0.05 '.' 0.1 ' ' 1.

Log-Likelihood: -131.46.

McFadden R<sup>2</sup>: 0.81.

Likelihood ratio test: chi-square = 1083.1 (p-value = < 2.22e-16).

optimized model, followed by the RF, MLP, and KNN models.

Estimated coefficients from the LR model were incorporated into equation (8) to generate the combined flood susceptibility map, which

was then categorized using the Quantile classification method into five classes (Fig. 6b). About 59.9% of the total study area was classified as being susceptible to flooding of moderate to very high severity. Most of these places were inundated during various historical flood events (Fig. 6a). The optimized FSM produced higher levels of spatial agreement, with correlation coefficients between the optimized FSM and all four models ranging from 0.76 (KNN and optimized model) to 0.92 (RF and optimized model) (Fig. 5).

### 3.4. Performance assessment of different FSMs

The results of the various performance indicators are shown in Fig. 7 and Table 3. All five models had very high prediction accuracy, with AUC values > 0.95. Among the four standalone and hybridized ML models, the RF model obtained the greatest AUC value of 0.984, followed by the hybridized GA – Gaussian RBF – SVR model (AUC – 0.983),

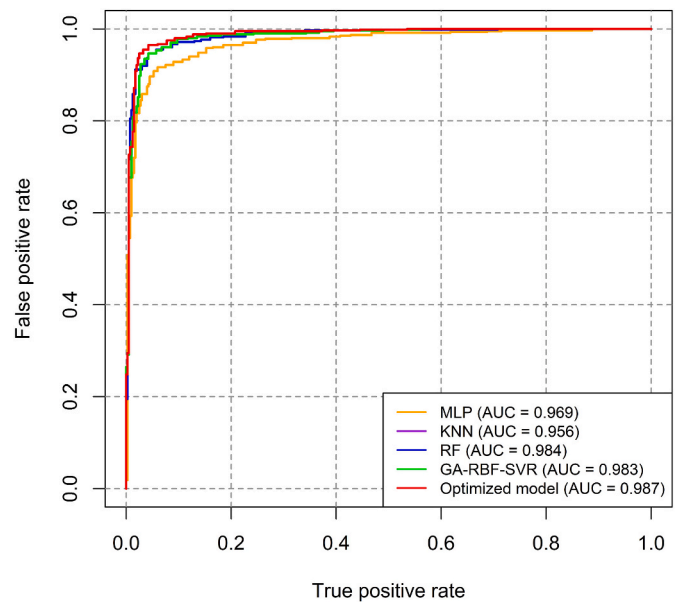


Fig. 7. Receiver operating characteristic (ROC) curves with corresponding values of area under the curves (AUC) of five models.

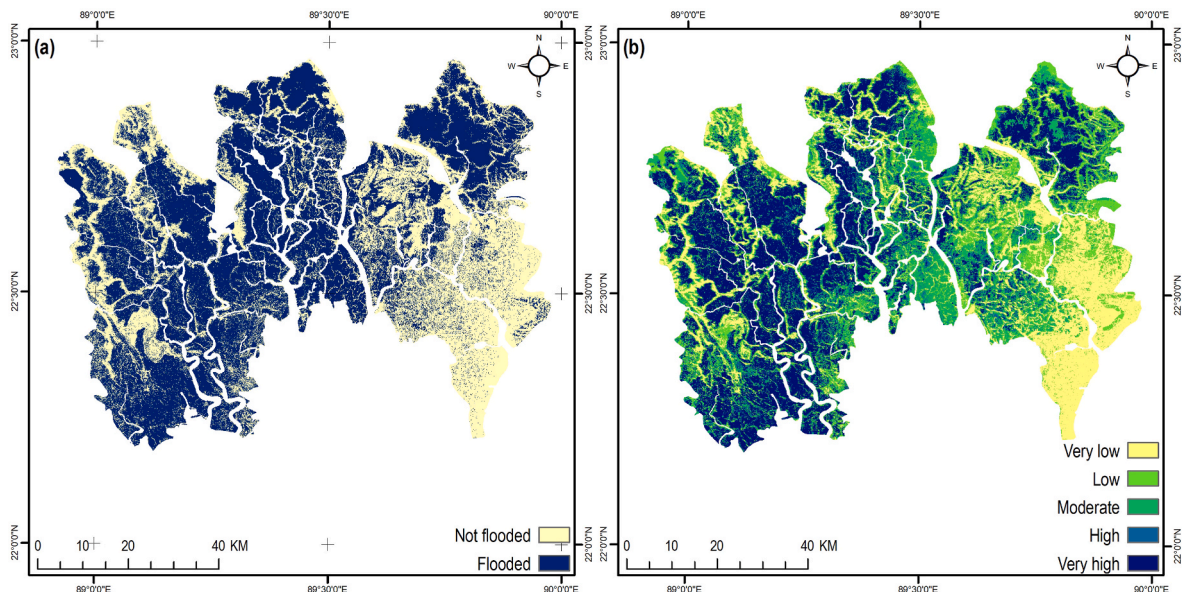


Fig. 6. (a) Inundation areas during historical flood events; and (b) simulated flood susceptible areas with optimized model.

**Table 3**  
Results of model performance assessment.

Models	AUC	Cut-off	Overall accuracy	Sensitivity	Specificity	Kappa coefficient	MSE
MLP	0.967	0.30	0.909	0.910	0.94	0.809	0.127
KNN	0.956	0.372	0.904	0.938	0.865	0.798	0.083
RF	0.984	0.476	0.942	0.937	0.957	0.879	0.064
GA-RBF-SVR	0.983	0.552	0.945	0.942	0.955	0.886	0.070
<b>Optimized model</b>	<b>0.987</b>	<b>0.628</b>	<b>0.957</b>	<b>0.945</b>	<b>0.973</b>	<b>0.911</b>	<b>0.035</b>

MLP (AUC – 0.969), and KNN (AUC – 0.956). The prediction accuracy of optimized FSM was greater, with an AUC value of 0.987 (Fig. 7).

While AUC values show how well the models performed generally, they do not reveal which particular classes were misclassified. To assess the performance and provide further insights into the relationship between observed and modeled flood and non-flood locations, a number of indices, including overall accuracy (OA), sensitivity, specificity, kappa coefficient, and mean squared error (MSE), were computed (Table 3). The RF model achieved the greatest OA value of 0.931 and the highest kappa statistic of 0.853 among the four ML models, while the hybridized GA – Gaussian RBF – SVR model came in second with an OA value of 0.924 and a kappa statistic of 0.840. Besides, the RF model achieved the lowest MSE value of 0.064, followed by the hybridized GA – Gaussian RBF – SVR model (MSE = 0.070). The KNN and MLP models performed less well compared to the other two models. Again, the optimized model improved the values of all performance assessment metrics.

### 3.5. Sensitivity analysis

This study investigated sensitivity of five flood susceptibility models to various flood causative factors using RF algorithm's %IncMSE and IncNodePurity scores. In general, all models were significantly impacted by surface elevation and the spatial pattern of land cover. A substantial degree of influence of precipitation was also observed. As model performance improved, the sensitivity of different models to flood indicators decreased. As a consequence, the optimized model had, the lowest values for %IncMSE and IncNodePurity for all flood causative factors when compared to the other four models (Fig. 8).

## 4. Discussion

Although GIS-based ML is a powerful tool for predicting natural hazards (such as floods, landslides, etc.), the results are subject to uncertainty because of model assumptions, the weighting of the criteria, and the quality and availability of the data (Rossi et al., 2010; Sterlacchini et al., 2011). There have only been a few attempts to overcome uncertainty in ML-based flood susceptibility models so far. This study sought to present an approach to minimize spatial disagreement in flood prediction using four sample standalone and hybridized ML algorithms: GA-RBF-SVR, RF, MLP, and KNN. The premise behind this work was that flood prediction does change geographically based on the model utilized. The outcomes of these four models were combined to create an optimum model. The study concentrated on the southwest embanked region of Bangladesh, which is prone to various types of recurring floods (Adnan et al., 2019).

The results of various models indicated that approximately 60% of the total land area is at risk of flooding. A number of recent studies produced results that were comparable (Adnan et al., 2019, 2020b). Despite obtaining similar extent of flood potential areas using various models, predictions were spatially heterogeneous. A comparison of the results of four different models revealed that the degree of model fit is not a reliable predictor of the model's ability to forecast floods. Pixel-wise correlation coefficients across various models ranged from 0.62 to 0.91. This study demonstrated that there exist uncertainties in ML-based flood prediction despite a high degree of prediction accuracy. This is because the degrees of influence of various flood conditioning

factors on the chance of flooding vary across different models. For instance, elevation was found to be the most influential factor in MLP, RF, and GA-RBF-SVR models, while land use was the most significant parameter in KNN model (Fig. 8). In addition, other flood conditioning factors such as precipitation, curvature, and soil permeability had considerable levels of influence. However, spatial variation of weights was observed. Feizizadeh and Kienberger (2017) suggested that determining uncertainties in GIS-based multicriteria decision analysis methods require a complete understanding of tradeoffs between various factors within a model.

All models produced very high prediction accuracy as indicated by model performance assessment indices, with the AUC values ranging from 0.956 (KNN) to 0.984 (RF). Many recent studies also ascertained the high accuracy of standalone and hybridized ML algorithm-based flood susceptibility models (Khosravi et al., 2019; Nachappa et al., 2020; Rahman et al., 2019; Siam et al., 2021, 2022). Although useful, the model performance assessment indicators cannot examine a model's efficacy and reliability in their whole (Guzzetti et al., 2006; Rossi et al., 2010). This study noted that an optimized model can improve flood prediction accuracy by minimizing the likelihood of spatial disagreement across various models. Combining the outputs of various ML-based models reduced the number of classification errors, compared to individual models (Fig. 7). Similar result was found in several studies (Ghorbanzadeh et al., 2018; Rossi et al., 2010). Additionally, the optimized models demonstrated a significantly lower variability in estimating susceptibility compared to the variability measured by the single models, indicating reduced uncertainties brought on by spatial disagreement (Guzzetti et al., 2006), thus guiding, more consistent flood susceptibility mapping. This is as a result of the improved FSM extracting the accurately determined flood and non-flood locations from each of the four models. The optimized model's assertion of lower variability is supported by improved spatial agreements (Fig. 5) and improved prediction accuracy (Fig. 7).

## 5. Conclusion

Predicting natural hazards such as floods is a challenging task due to complex interactions among various causative factors. The focus of many recent studies was to select a suitable method for predicting flood hazards (Bui et al., 2019; Chen et al., 2020; Khosravi et al., 2019; Nachappa et al., 2020; Tehrany et al., 2019). Flood prediction maps developed based on sample flood inventory data could create uncertainties in its spatial prediction pattern. A few studies attempted to analyze uncertainties in multi-criteria decision analysis-based flood susceptibility modeling (de Brito et al., 2019; Feizizadeh and Kienberger, 2017; Ghorbanzadeh et al., 2018). The variability in the spatial pattern that the ML-based FSM predict, however, has not received much attention. This study proposed an approach to enhance the geographical agreement of flood susceptibility across four ML-based FSMs: Multilayer perceptron (MLP), k-nearest neighbor (KNN), random forest (RF), and hybridized genetic algorithm-gaussian radial basis function-support vector regression (GA-RBF-SVR) models. The models were developed in the southwestern coastal region of Bangladesh. The outcomes showed that the RF model outperforms the other three, producing the highest prediction accuracy. But it was discovered that the flood predictions made by such models varied pixel by pixel. By combining the results of

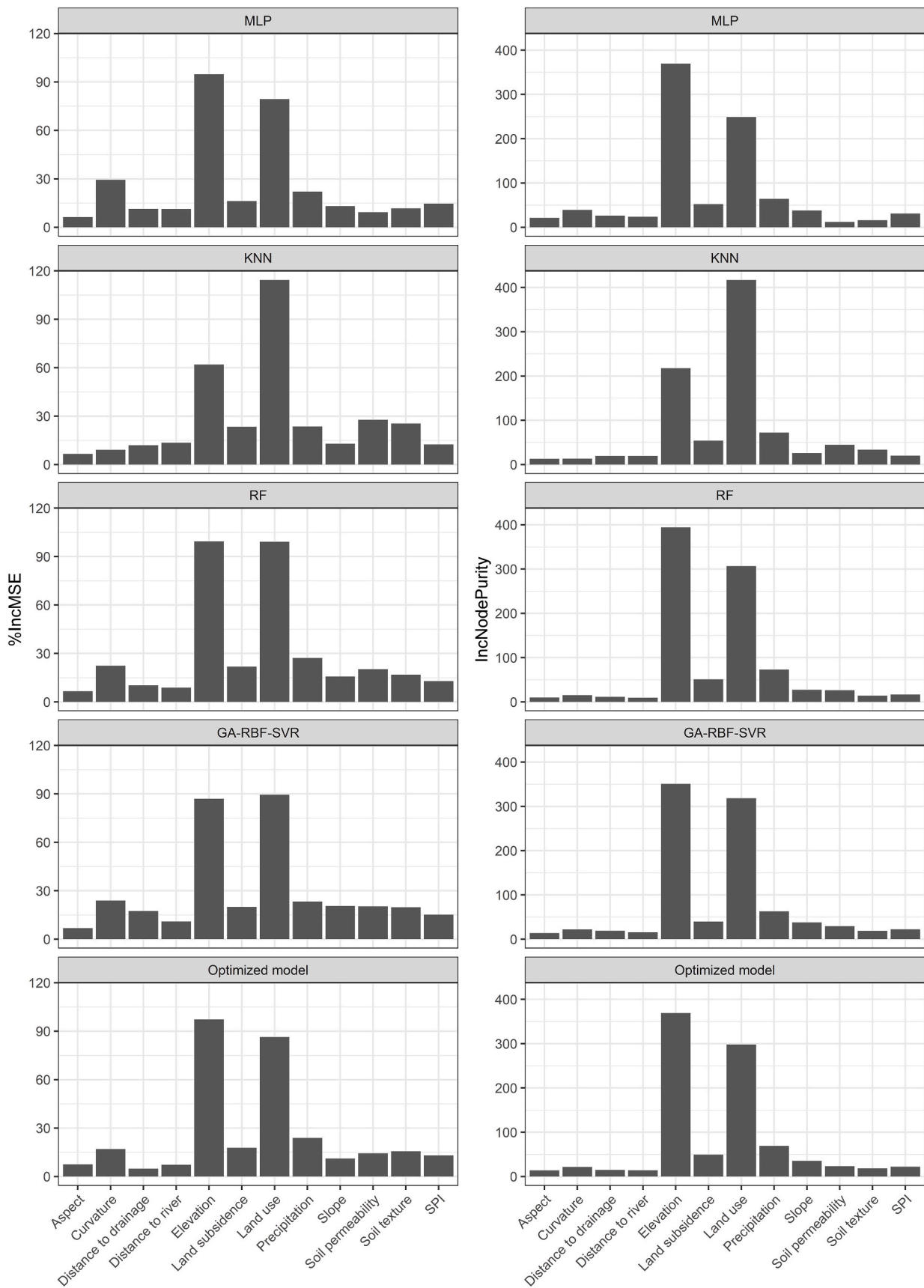


Fig. 8. Sensitivity of flood susceptibility models to flood causative factors, based on %IncMSE and IncNodePurity.

four models, an improved FSM was created to reduce such uncertainty in the predicted spatial pattern. When compared to the individual models, the optimized model had better spatial agreement and more accurate flood predictions, according to the models' performance assessment metrics.

Despite improving flood predictions, there are still certain areas where this study may be strengthened. For instance, flood inventory data used in this study was developed by analyzing the Landsat satellite images and validated through fieldwork (Adnan et al., 2020b). Due to the unavailability of cloud-free images during the monsoon season, flood maps were produced by comparing pre- and post-monsoon images (Adnan et al., 2019). The Synthetic-aperture radar (SAR) dataset, however, may allow for flood observation and the identification of inundation zones during the monsoon seasons. The sampling methodology utilized for both the model's training and testing represents another drawback. Different training and testing datasets are produced each time random sampling is utilized. As a result, the models generated using these datasets may differ. The optimal model can be chosen by repeatedly using the random sampling method to address this issue (Ahmadlou et al., 2021). In addition, the accuracy of the FSM depends on the input parameters used, especially the DEM. The 30-m resolution ALOS DEM of was used since it has reasonably low root-mean-square error (1.78 m) in vertical accuracy among the freely accessible DEMs (Hasan et al., 2020). High-resolution DEM use, however, could enhance the FSMs.

Although there are certain drawbacks, the framework presented in this study may help water resources managers and policymakers create risk-based development strategies. A similar modeling framework may be used to other areas that are vulnerable to floods brought on by anthropogenic activity and climate change. In comparison to the current ML-based modeling techniques, the proposed optimized flood susceptibility model represents an improvement. The results of this study could be used to develop flood early warning systems in Bangladesh (Siam et al., 2022), supporting the improvement of the nation's catastrophe resilience.

#### Credit author statement

**Adnan, M. S. G.:** Conceptualization, Methodology, Software, Formal analysis, Validation, Writing - Original Draft, Writing - Review & Editing, Visualization; **Zakaria, S. S.:** Methodology, Formal analysis, Software; **Kabir, I.:** Data curation, Writing - Original Draft, Visualization; **Kabir, Z.:** Investigation, Resources, Software; **Ahmed, M. R.:** Investigation, Resources, Funding acquisition; **Hassan, Q. K.:** Investigation, Resources, Funding acquisition; **Rahman, R. M.:** Investigation, Validation, Funding acquisition; **Dewan, A.:** Conceptualization, Supervision, Validation.

#### Declaration of competing interest

The authors declare that they have no known competing financial interests or personal relationships that could have appeared to influence the work reported in this paper.

#### Data availability

Data will be made available on request.

#### Acknowledgements

This work is partly supported by the Ministry of Post, Telecommunication and Information Technology, Bangladesh through ICT Innovation Fund (2020–21) round 3: Grant Number 12.

#### Appendix A. Supplementary data

Supplementary data to this article can be found online at <https://doi.org/10.1016/j.jenvman.2022.116813>.

#### References

- Adnan, M.S.G., Haque, A., Hall, J.W., 2019. Have coastal embankments reduced flooding in Bangladesh? *Sci. Total Environ.* 682, 405–416.
- Adnan, M.S.G., Rahman, M.S., Ahmed, N., Ahmed, B., Rabbi, M., Rahman, R.M., 2020a. Improving spatial agreement in machine learning-based landslide susceptibility mapping. *Rem. Sens.* 12, 3347.
- Adnan, M.S.G., Talchabhadel, R., Nakagawa, H., Hall, J.W., 2020b. The potential of tidal river management for flood alleviation in south western Bangladesh. *Sci. Total Environ.* 731, 138747.
- Ahmadlou, M., Al-Fugara, A.K., Al-Shabeeb, A.R., Arora, A., Al-Adamat, R., Pham, Q.B., Al-Ansari, N., Linh, N.T.T., Sajedi, H., 2021. Flood susceptibility mapping and assessment using a novel deep learning model combining multilayer perceptron and autoencoder neural networks. *J. Flood Risk Manag.* 14, e12683.
- Al-Juaidi, A.E., Nassar, A.M., Al-Juaidi, O.E., 2018. Evaluation of flood susceptibility mapping using logistic regression and GIS conditioning factors. *Arabian J. Geosci.* 11, 1–10.
- Ali, L., 2002. An Integrated Approach for the Improvement of Flood Control and Drainage Schemes in the Coastal Belt of Bangladesh. Wageningen University and Research.
- Ali, S.A., Parvin, F., Pham, Q.B., Vojtek, M., Vojteková, J., Costache, R., Linh, N.T.T., Nguyen, H.Q., Ahmad, A., Ghorbani, M.A., 2020. GIS-based comparative assessment of flood susceptibility mapping using hybrid multi-criteria decision-making approach, naive Bayes tree, bivariate statistics and logistic regression: a case of Topľa basin, Slovakia. *Ecol. Indicat.* 117, 106620.
- Apel, H., Aronica, G., Kreibich, H., Thielen, A., 2009. Flood risk analyses—how detailed do we need to be? *Nat. Hazards* 49, 79–98.
- Ardiclioglu, M., Hadi, A.M., Periku, E., Kuriqi, A., 2022. Experimental and numerical investigation of bridge configuration effect on hydraulic regime. *Int. J. Civ. Eng.* 1–11.
- Auerbach, L., Goodbred Jr., S., Mondal, D., Wilson, C., Ahmed, K., Roy, K., Steckler, M., Small, C., Gilligan, J., Ackerly, B., 2015. Flood risk of natural and embanked landscapes on the Ganges–Brahmaputra tidal delta plain. *Nat. Clim. Change* 5, 153–157.
- Avand, M., Kuriqi, A., Khazaei, M., Ghorbanzadeh, O., 2022. DEM resolution effects on machine learning performance for flood probability mapping. *J. Hydro-environ. Res.* 40, 1–16.
- Bannari, A., Ghadeer, A., El-Battay, A., Hameed, N., Rouai, M., 2017. Detection of Areas Associated with Flash Floods and Erosion Caused by Rainfall Storm Using Topographic Attributes, Hydrologic Indices, and GIS. *Global Changes and Natural Disaster Management: Geo-Information Technologies*. Springer, pp. 155–174.
- Batar, A.K., Watanabe, T., 2021. Landslide susceptibility mapping and assessment using geospatial platforms and weights of evidence (WoE) method in the Indian Himalayan Region: recent developments, gaps, and future directions. *ISPRS Int. J. Geo-Inf.* 10, 114.
- Bondarenko, M., Kerr, D., Sorichetta, A., Tatem, A.J., 2020. In: *WorldPop, U.o.S. (Ed.), Census/projection-disaggregated Gridded Population Datasets for 189 Countries in 2020 Using Built-Settlement Growth Model (BSGM) Outputs (UK)*.
- Breiman, L., 2001. Random forests. *Mach. Learn.* 45, 5–32.
- Brown, S., Nicholls, R.J., 2015. Subsidence and human influences in mega deltas: the case of the Ganges–Brahmaputra–Meghna. *Sci. Total Environ.* 527, 362–374.
- Brunner, G.W., 1995. HEC-RAS River Analysis System. Hydraulic Reference Manual. Hydrologic Engineering Center Davis CA. Version 1.0.
- Bui, D.T., Ngo, P.-T.T., Pham, T.D., Jaafari, A., Minh, N.Q., Hoa, P.V., Samui, P., 2019. A novel hybrid approach based on a swarm intelligence optimized extreme learning machine for flash flood susceptibility mapping. *Catena* 179, 184–196.
- Bui, D.T., Pradhan, B., Nampak, H., Bui, Q.-T., Tran, Q.-A., Nguyen, Q.-P., 2016. Hybrid artificial intelligence approach based on neural fuzzy inference model and metaheuristic optimization for flood susceptibility modeling in a high-frequency tropical cyclone area using GIS. *J. Hydrol.* 540, 317–330.
- Chen, W., Li, Y., Xue, W., Shahabi, H., Li, S., Hong, H., Wang, X., Bian, H., Zhang, S., Pradhan, B., 2020. Modeling flood susceptibility using data-driven approaches of naive bayes tree, alternating decision tree, and random forest methods. *Sci. Total Environ.* 701, 134979.
- Costache, R., 2019. Flash-flood Potential Index mapping using weights of evidence, decision Trees models and their novel hybrid integration. *Stoch. Environ. Res. Risk Assess.* 33, 1375–1402.
- Cover, T., Hart, P., 1967. Nearest neighbor pattern classification. *IEEE Trans. Inf. Theor.* 13, 21–27.
- Crosetto, M., Tarantola, S., Saltelli, A., 2000. Sensitivity and uncertainty analysis in spatial modelling based on GIS. *Agric. Ecosyst. Environ.* 81, 71–79.
- Dasgupta, A., Grimaldi, S., Ramsankaran, R., Pauwels, V.R., Walker, J.P., 2018. Towards operational SAR-based flood mapping using neuro-fuzzy texture-based approaches. *Rem. Sens. Environ.* 215, 313–329.
- de Brito, M.M., Almoradie, A., Evers, M., 2019. Spatially-explicit sensitivity and uncertainty analysis in a MCDA-based flood vulnerability model. *Int. J. Geogr. Inf. Sci.* 33, 1788–1806.
- Dewan, Ashraf, Kankam-Yeboah, Kwabena, Nishigaki, Makoto, 2006. Using synthetic aperture radar (SAR) data for mapping river water flooding in an urban landscape: a

- case study of Greater Dhaka, Bangladesh. *J. Jpn. Soc. Hydrol. Water Resour.* 19 (1) <https://doi.org/10.3178/jjshwr.19.44>.
- Di Baldassarre, G., Schumann, G., Bates, P.D., Freer, J.E., Beven, K.J., 2010. Flood-plain mapping: a critical discussion of deterministic and probabilistic approaches. *Hydrol. Sci. J.-J. Sci. Hydrol.* 55, 364–376.
- Di Baldassarre, G., Viglione, A., Carr, G., Kuil, L., Salinas, J., Blöschl, G., 2013. Socio-hydrology: conceptualising human-flood interactions. *Hydrol. Earth Syst. Sci.* 17, 3295–3303.
- El-Haddad, B.A., Youssef, A.M., Pourghasemi, H.R., Pradhan, B., El-Shater, A.-H., El-Khashab, M.H., 2021. Flood susceptibility prediction using four machine learning techniques and comparison of their performance at Wadi Qena Basin, Egypt. *Nat. Hazards* 105, 83–114.
- Falah, F., Rahmati, O., Rostami, M., Ahmadisharaf, E., Daliakopoulos, I.N., Pourghasemi, H.R., 2019. Artificial Neural Networks for Flood Susceptibility Mapping in Data-Scarce Urban Areas, Spatial Modeling in GIS and R for Earth and Environmental Sciences. Elsevier, pp. 323–336.
- Feizizadeh, B., Kienberger, S., 2017. Spatially explicit sensitivity and uncertainty analysis for multicriteria-based vulnerability assessment. *J. Environ. Plann. Manag.* 60, 2013–2035.
- Ghorbanzadeh, O., Feizizadeh, B., Blaschke, T., 2018. Multi-criteria risk evaluation by integrating an analytical network process approach into GIS-based sensitivity and uncertainty analyses. *Geomatics, Nat. Hazards Risk* 9, 127–151.
- Guzzetti, F., Reichenbach, P., Ardizzone, F., Cardinali, M., Galli, M., 2006. Estimating the quality of landslide susceptibility models. *Geomorphology* 81, 166–184.
- Hag, M., Akhtar, M., Muhammad, S., Paras, S., Rahmatullah, J., 2012. Techniques of remote sensing and GIS for flood monitoring and damage assessment: a case study of Sindh province, Pakistan. *Egypt. J. Remote Sens. Space Sci.* 15, 135–141.
- Haque, A., Kay, S., Nicholls, R.J., 2018. Present and future fluvial, tidal and storm surge flooding in coastal Bangladesh. In: *Ecosystem Services for Well-Being in Deltas*. Palgrave Macmillan, Cham, pp. 293–314.
- Hasan, M.K., Kumar, L., Gopalakrishnan, T., 2020. Inundation modelling for Bangladeshi coasts using downscaled and bias-corrected temperature. *Climate Risk Manag.* 27, 100207.
- He, Q.P., Wang, J., 2007. Fault detection using the k-nearest neighbor rule for semiconductor manufacturing processes. *IEEE Trans. Semicond. Manuf.* 20, 345–354.
- Hui, R., Jachens, E., Lund, J., 2016. Risk-based planning analysis for a single levee. *Water Resour. Res.* 52, 2513–2528.
- Islam, A.R.M.T., Talukdar, S., Mahato, S., Kundu, S., Eibek, K.U., Pham, Q.B., Kuriqi, A., Linh, N.T.T., 2021. Flood susceptibility modelling using advanced ensemble machine learning models. *Geosci. Front.* 12, 101075.
- JAXA, 2015. ALOS Global Digital Surface Model “ALOS World 3D-30m”(AW3D30).
- Kalantar, B., Ueda, N., Saeidi, V., Janizadeh, S., Shabani, F., Ahmadi, K., Shabani, F., 2021. Deep neural network utilizing remote sensing datasets for flood hazard susceptibility mapping in Brisbane, Australia. *Rem. Sens.* 13, 2638.
- Khosravi, K., Shahabi, H., Pham, B.T., Adamowski, J., Shirzadi, A., Pradhan, B., Dou, J., Ly, H.-B., Gróf, G., Ho, H.L., 2019. A comparative assessment of flood susceptibility modeling using multi-criteria decision-making analysis and machine learning methods. *J. Hydrol.* 573, 311–323.
- Kia, M.B., Pirasteh, S., Pradhan, B., Mahmud, A.R., Sulaiman, W.N.A., Moradi, A., 2012. An artificial neural network model for flood simulation using GIS: Johor River Basin, Malaysia. *Environ. Earth Sci.* 67, 251–264.
- Kjeldsen, T.R., 2010. Modelling the impact of urbanization on flood frequency relationships in the UK. *Nord. Hydrol.* 41, 391–405.
- Kumar, M., Kumar, P., Kumar, A., Elbeltagi, A., Kuriqi, A., 2022. Modeling stage-discharge-sediment using support vector machine and artificial neural network coupled with wavelet transform. *Appl. Water Sci.* 12, 1–21.
- Lee, S., Kim, J.-C., Jung, H.-S., Lee, M.J., Lee, S., 2017. Spatial prediction of flood susceptibility using random-forest and boosted-tree models in Seoul metropolitan city, Korea. *Geomatics, Nat. Hazards Risk* 8, 1185–1203.
- Liu, K., Li, Z., Yao, C., Chen, J., Zhang, K., Saifullah, M., 2016. Coupling the k-nearest neighbor procedure with the Kalman filter for real-time updating of the hydraulic model in flood forecasting. *Int. J. Sediment Res.* 31, 149–158.
- Löwe, R., Böhm, J., Jensen, D.G., Leandro, J., Rasmussen, S.H., 2021. U-FLOOD—Topographic deep learning for predicting urban pluvial flood water depth. *J. Hydrol.* 603, 126898.
- Malik, S., Pal, S.C., 2021. Application of 2D numerical simulation for rating curve development and inundation area mapping: a case study of monsoon dominated Dwarakeswar river. *Int. J. River Basin Manag.* 19, 553–563.
- Mansur, A.V., Brondizio, E.S., Roy, S., de Miranda Araújo Soares, P.P., Newton, A., 2018. Adapting to urban challenges in the Amazon: flood risk and infrastructure deficiencies in Belém, Brazil. *Reg. Environ. Change* 18, 1411–1426.
- Midi, H., Sarkar, S.K., Rana, S., 2010. Collinearity diagnostics of binary logistic regression model. *J. Interdiscipl. Math.* 13, 253–267.
- Mirza, M.Q., Ericksen, N.J., 1996. Impact of water control projects on fisheries resources in Bangladesh. *Environ. Manag.* 20, 523–539.
- Montz, B.E., Tobin, G.A., 2008. Livin’ large with levees: lessons learned and lost. *Nat. Hazards Rev.* 9, 150–157.
- Msabi, M.M., Makonyo, M., 2021. Flood susceptibility mapping using GIS and multi-criteria decision analysis: a case of Dodoma region, central Tanzania. *Remote Sens. Appl.: Soc. Environ.* 21, 100445.
- Mukhopadhyay, A., Hornby, D.D., Hutton, C.W., Lázár, A.N., Amoako Johnson, F., Ghosh, T., 2018. Land Cover and Land Use Analysis in Coastal Bangladesh, Ecosystem Services for Well-Being in Deltas. Palgrave Macmillan, Cham, pp. 367–381.
- Muñoz, D.F., Yin, D., Bakhtyar, R., Moftakhari, H., Xue, Z., Mandli, K., Ferreira, C., 2021. Inter-model Comparison of Delft3D-FM and 2D HEC-RAS for Total Water Level Prediction in Coastal to Inland Transition Zones. *JAWRA Journal of the American Water Resources Association*.
- Murtagh, F., 1991. Multilayer perceptrons for classification and regression. *Neurocomputing* 2, 183–197.
- Nachappa, T.G., Piralilou, S.T., Gholamnia, K., Ghorbanzadeh, O., Rahmati, O., Blaschke, T., 2020. Flood susceptibility mapping with machine learning, multi-criteria decision analysis and ensemble using Dempster Shafer Theory. *J. Hydrol.* 590, 125275.
- Papaioannou, G., Efstratiadis, A., Vasilades, L., Loukas, A., Papalexioiu, S.M., Koukouvinos, A., Tsoukalas, I., Kossieris, P., 2018. An operational method for flood directive implementation in ungauged urban areas. *Hydrology* 5, 24.
- Pham, B.T., Luu, C., Van Dao, D., Van Phong, T., Nguyen, H.D., Van Le, H., von Meding, J., Prakash, I., 2021. Flood risk assessment using deep learning integrated with multi-criteria decision analysis. *Knowl. Base Syst.* 219, 106899.
- Poussin, J.K., Botzen, W.W., Aerts, J.C., 2015. Effectiveness of flood damage mitigation measures: empirical evidence from French flood disasters. *Global Environ. Change* 31, 74–84.
- Rahman, M., Ningsheng, C., Islam, M.M., Dewan, A., Iqbal, J., Washakh, R.M.A., Shufeng, T., 2019. Flood susceptibility assessment in Bangladesh using machine learning and multi-criteria decision analysis. *Earth Syst. Environ.* 3, 585–601.
- Rezaeianzadeh, M., Tabari, H., Arabi Yazdi, A., Isik, S., Kalin, L., 2014. Flood flow forecasting using ANN, ANFIS and regression models. *Neural Comput. Appl.* 25, 25–37.
- Rossi, M., Guzzetti, F., Reichenbach, P., Mondini, A.C., Peruccacci, S., 2010. Optimal landslide susceptibility zonation based on multiple forecasts. *Geomorphology* 114, 129–142.
- Saha, T.K., Pal, S., Talukdar, S., Debanshi, S., Khatun, R., Singha, P., Mandal, I., 2021. How far spatial resolution affects the ensemble machine learning based flood susceptibility prediction in data sparse region. *J. Environ. Manag.* 297, 113344.
- Sarker, C., Mejias, L., Maire, F., Woodley, A., 2019. Flood mapping with convolutional neural networks using spatio-contextual pixel information. *Rem. Sens.* 11, 2331.
- Shafizadeh-Moghadam, H., Valavi, R., Shahabi, H., Chapi, K., Shirzadi, A., 2018. Novel forecasting approaches using combination of machine learning and statistical models for flood susceptibility mapping. *J. Environ. Manag.* 217, 1–11.
- Shahabi, H., Shirzadi, A., Ghaderi, K., Omidvar, E., Al-Ansari, N., Clague, J.J., Geertsema, M., Khosravi, K., Amini, A., Bahrami, S., 2020. Flood detection and susceptibility mapping using sentinel-1 remote sensing data and a machine learning approach: hybrid intelligence of bagging ensemble based on k-nearest neighbor classifier. *Rem. Sens.* 12, 266.
- Shirzadi, A., Asadi, S., Shahabi, H., Ronoud, S., Clague, J.J., Khosravi, K., Pham, B.T., Ahmad, B.B., Bui, D.T., 2020. A novel ensemble learning based on Bayesian Belief Network coupled with an extreme learning machine for flash flood susceptibility mapping. *Eng. Appl. Artif. Intell.* 96, 103971.
- Siam, Z.S., Hasan, R.T., Anik, S.S., Noor, F., Adnan, M.S.G., Rahman, R.M., 2021. Study of Hybridized Support Vector Regression Based Flood Susceptibility Mapping for Bangladesh, International Conference on Industrial, Engineering and Other Applications of Applied Intelligent Systems. Springer, pp. 59–71.
- Siam, Z.S., Hasan, R.T., Anik, S.S., Noor, F., Adnan, M.S.G., Rahman, R.M., Dewan, A., 2022. National-Scale flood risk assessment using GIS and remote sensing-based hybridized deep neural network and fuzzy analytic hierarchy process models: a case of Bangladesh. *Geocarto Int.* 1–28.
- Sterlacchini, S., Ballabio, C., Blahut, J., Masetti, M., Sorichetta, A., 2011. Spatial agreement of predicted patterns in landslide susceptibility maps. *Geomorphology* 125, 51–61.
- Tehrany, M.S., Kumar, L., Shabani, F., 2019. A novel GIS-based ensemble technique for flood susceptibility mapping using evidential belief function and support vector machine: brisbane, Australia. *PeerJ* 7, e7653.
- Tehrany, M.S., Lee, M.-J., Pradhan, B., Jebur, M.N., Lee, S., 2014a. Flood susceptibility mapping using integrated bivariate and multivariate statistical models. *Environ. Earth Sci.* 72, 4001–4015.
- Tehrany, M.S., Pradhan, B., Jebur, M.N., 2013. Spatial prediction of flood susceptible areas using rule based decision tree (DT) and a novel ensemble bivariate and multivariate statistical models in GIS. *J. Hydrol.* 504, 69–79.
- Tehrany, M.S., Pradhan, B., Jebur, M.N., 2014b. Flood susceptibility mapping using a novel ensemble weights-of-evidence and support vector machine models in GIS. *J. Hydrol.* 512, 332–343.
- Tralli, D.M., Blom, R.G., Zlotnicki, V., Donnellan, A., Evans, D.L., 2005. Satellite remote sensing of earthquake, volcano, flood, landslide and coastal inundation hazards. *ISPRS J. Photogrammetry Remote Sens.* 59, 185–198.
- Vojtek, M., Vojteková, J., 2019. Flood susceptibility mapping on a national scale in Slovakia using the analytical hierarchy process. *Water* 11, 364.
- Wang, Y., Hong, H., Chen, W., Li, S., Pamucar, D., Gigović, L., Drobnjak, S., Tien Bui, D., Duan, H., 2019. A hybrid GIS multi-criteria decision-making method for flood susceptibility mapping at Shangyou, China. *Rem. Sens.* 11, 62.
- Warner, J.F., van Staveren, M.F., van Tatenhove, J., 2018. Cutting dikes, cutting ties? Reintroducing flood dynamics in coastal polders in Bangladesh and The Netherlands. *Int. J. Disaster Risk Reduc.* 32, 106–112.
- WARPO, 2018. National water resources database (NWRD). In: *WARPO*, W.R.P.O. (Ed.), Dhaka, Bangladesh.
- Yariyan, P., Avand, M., Abbaspour, R.A., Torabi Haghighi, A., Costache, R., Ghorbanzadeh, O., Janizadeh, S., Blaschke, T., 2020. Flood susceptibility mapping using an improved analytic network process with statistical models. *Geomatics, Nat. Hazards Risk* 11, 2282–2314.
- Youden, W.J., 1950. Index for rating diagnostic tests. *Cancer* 3, 32–35.

- Youssef, A.M., Pradhan, B., Hassan, A.M., 2011. Flash flood risk estimation along the St. Katherine road, southern Sinai, Egypt using GIS based morphometry and satellite imagery. *Environ. Earth Sci.* 62, 611–623.
- Zhao, G., Pang, B., Xu, Z., Peng, D., Xu, L., 2019. Assessment of urban flood susceptibility using semi-supervised machine learning model. *Sci. Total Environ.* 659, 940–949.
- Zhou, Q., Mikkelsen, P.S., Halsnaes, K., Arnbjerg-Nielsen, K., 2012. Framework for economic pluvial flood risk assessment considering climate change effects and adaptation benefits. *J. Hydrol.* 414, 539–549.
- Zhu, Z., Zhang, Y., 2022. Flood disaster risk assessment based on random forest algorithm. *Neural Comput. Appl.* 34, 3443–3455.